Estimation of Sub-Canopy Ground Height from Capon TomoSAR profiles: A Performance Analysis

Matteo Pardini[a], Konstantinos P. Papathanassiou[a]
[a] German Aerospace Center (DLR), Microwave and Radar Institute (HR), Wessling (Germany) – matteo.pardini@dlr.de

Abstract

Synthetic Aperture Radar (SAR) waves at low frequency can penetrate through the different forest layers down to the ground. The received signal contains information not only on the 3-D distribution of the vegetation scatterers, but also on the underlying ground. Using multiple acquisitions, SAR tomographic (TomoSAR) techniques estimate vertical reflectivity profiles, thus they enable the separation and localization of multiple backscattering contributions. The objective of this paper is to discuss the capabilities of the Capon TomoSAR profiles in the estimation of the sub-canopy ground height by addressing the role of the TomoSAR acquisition configuration, the ground-to-volume ratio and the volume reflectivity profiles. The analysis is carried out by means of theoretical relationships and supported by airborne real L-band TomoSAR data acquired over a temperate forest site in the south of Germany.

1 Introduction

With decreasing frequency, Synthetic Aperture Radar (SAR) pulses penetrate more and more into and through forest volumes, and interact with vegetation elements located at different heights and with the underlying ground. The sensitivity to the ground scattering makes possible its localization. SAR Tomography (TomoSAR) techniques rely on the angular diversity of multiple SAR images acquired under slightly different incidence angles (e.g., along displaced tracks or orbits) to estimate the 3-D distribution of the backscattered power, also known as the 3-D radar reflectivity. Thus, TomoSAR techniques can separate different scattering contributions, and in this way enable the estimation of the ground height as well. Accurate ground height estimates can be used not only for sub-canopy topography retrieval, but also for forest height estimation [1], and in the separation of ground and volume scattering (interferometric coherences and polarimetric covariances) [2], [3].

Several TomoSAR-based techniques have been developed and experimented at both P- and L-band for estimating the ground height. Besides model- or sparsity-based separation techniques [4]-[6], estimation procedures based on the identification of the ground scatterer in TomoSAR profiles have been considered [7]-[10]. In the latter case, it has been experimentally seen that simple empirical criteria can be followed, often obtaining accurate estimates with a low computational cost. Not only, but TomoSAR direct imaging algorithms overcome the ambiguity intrinsic in the separation between ground and volume scattering [2], [3]. However, at present there is no systematic assessment of the estimation performance achievable by the different algorithms, and of the related trade-offs and dependencies in terms of acquisition characteristics.

In this paper, the estimation of the sub-canopy ground height by using Capon TomoSAR profiles is considered. The objective is to analyse their estimation capabilities by addressing first of all the role of the characteristics of the TomoSAR acquisition. The benefit of the availability of multiple polarization channels is discussed as well. Performance dependencies on the scattering properties are considered, including the effects of different levels of ground-to-volume ratios and of the volume reflectivity profiles. Finally, the impact of the ground identification methodology on the estimation performance is assessed. The analysis is carried out by means of theoretical relationships derived in closed forms where possible. Real data results obtained by processing an airborne real L-band TomoSAR acquisition over a temperate forest site in the south of Germany are used to support the theoretical conclusions.

2 Methodology and theoretical relationships

In the following it is assumed that a TomoSAR acquisition in a fixed polarimetric channel is composed by K images. The steering vector $\mathbf{a}(z)$ contains the height-dependent phase (difference) with respect to a generic height z for each of the tracks. Its $k-$th $(k=1,\ldots,K)$ element is $\left[\mathbf{a}(z)\right]_k = \exp\{jk_{Z,k}z\}$, where $k_{Z,k}$ is the vertical wavenumber associated to the $k-$th image with respect to the reference (master) track [1]. For a fixed range-azimuth coordinate, the corresponding pixel amplitudes in the different images are collected in the K-dimensional vector $\mathbf{y}$. The associated TomoSAR covariance matrix is $\mathbf{R} := E\left\{\mathbf{y}\mathbf{y}^H\right\}$, where $E\{\cdot\}$ indicates the statistical expectation operator. Under the two-layer model (after coregistration, flat-Earth phase compensation, phase calibration, and spectral shift filtering), the coherence matrix $\mathbf{\Gamma}$ associated to $\mathbf{R}$ can be written as [1]-[3]:

$$\mathbf{\Gamma} = \frac{\mu}{1+\mu}\mathbf{\Gamma}_G + \frac{1}{1+\mu}\mathbf{\Gamma}_V \qquad (1)$$

where $\mathbf{\Gamma}_G$ and $\mathbf{\Gamma}_V$ are the coherence matrices of the ground and the volume scatterers, respectively, and μ is the ground-to-volume power ratio [1]. $\mathbf{\Gamma}_V$ is related to the volume reflectivity profile by means of a Fourier relationship [1]. It is assumed that the ground reflectivity is described by a Dirac-δ function, thus $\mathbf{\Gamma}_G := \mathbf{a}(z_0)\mathbf{a}^H(z_0)$ where z_0 is the unknown ground height [1].

The Capon estimate $P_C(z)$ of the reflectivity profile corresponding to $\mathbf{\Gamma}$ can be written as:

$$P_C(z) = K / [\mathbf{a}^H(z)\mathbf{\Gamma}^{-1}\mathbf{a}(z)] . \tag{2}$$

Under the assumptions above, and for a sufficient TomoSAR resolution, the ground scatterer appears as a peak in $P_C(z)$. Even for a very large number of looks, the estimation of the ground height from the location of the related peak is subject to an error that can be approximated as [12]:

$$\Delta z_0 \approx -P_C'(z_0) / P_C''(z_0) . \tag{3}$$

$P_C'(z_0)$ and $P_C''(z_0)$ are the first and second order derivatives of $P_C(z)$, respectively, around z_0. It can be demonstrated that Δz_0 depends on μ, and on the Capon profile $P_{CV}(z)$ of the volume scatterer and its derivatives around z_0.

In practical applications, the ground peak must be found among volume peaks and sidelobes within the same Capon profile. Although there is no established rule, the peak at the lowest height within a height interval is commonly identified as the ground scatterer [9], [10]. Both the retrieval of a meaningful height interval, and the possibility to mistake a sidelobes or a volume peak for the ground one concur to define the final estimation performance.

A meaningful height interval is typically retrieved by considering the scattering contributions for which $P_C(z) > T$. By inserting (1) in (2), it is possible to find that the ground contribution is selected if $\mu \geq \mu_{\min}$ with

$$\mu_{\min} = \frac{T - P_{CV}(z_0)}{K - 1} . \tag{4}$$

The choice of a suitable threshold T is a critical step. For instance, it can be observed that $T = 1$ is the minimum threshold that allows to detect a ground scatterer embedded in white noise (e.g. bare areas). This value can be retained also for forest areas, although no optimality is guaranteed. In **Figure 1** the values assumed by $\mu_{\min}$ as a function of $P_{CV}(z_0)$ are plotted for different values of the number of images K and $T = 1$. For any value of K, $\mu_{\min}$ decreases at the increase of $P_{CV}(z_0)$. At the same time, for any value of $P_{CV}(z_0)$ between 0 and 1, the presence of weaker ground scatterers can be detected by increasing K. In the limit case $P_{CV}(z_0) = 1$, it results $\mu_{\min} = 0$ regardless of K. In this case, the ground can be located just because the volume Capon profile exceeds the threshold at that height, independently of the "visibility" of the ground scattering. It is worth noting that under a Random-Volume-over-Ground assumption, multiple polarization channels can be used to maximise μ. Therefore, as the corresponding $\mu_{\min}$ increases, a lower number of acquisitions can be employed.

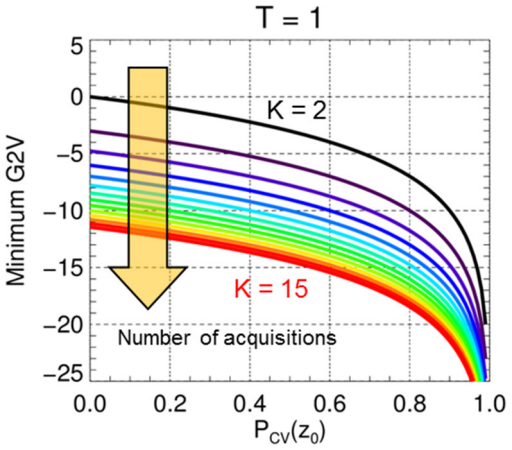

Figure 1 Behaviour of $\mu_{\min}$ as a function of $P_{CV}(z_0)$ and for different values of K.

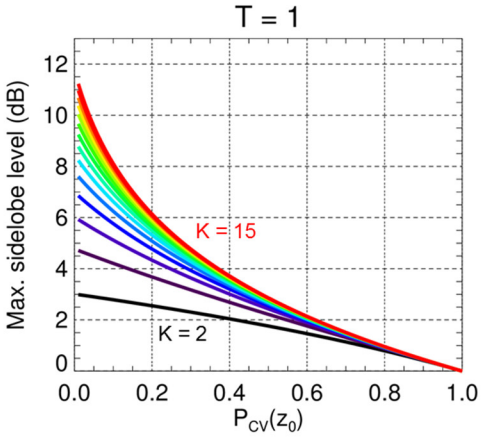

Figure 2 Required $P_{CV,\max} / P_{CV}(z_0)$ as a function of $P_{CV}(z_0)$ for different values of K, $T = 1$ and $\mu = \mu_{\min}$.

Assuming that a meaningful height interval has been retrieved, it is of interest to determine under which condition sidelobes and volume peaks are not mistaken for the ground scatterer, i.e. $P_C(z) < 1$. After some algebraic manipulations, it can be found that a sufficient condition is $P_{CV}(z) < P_{CV,\max}$, with

$$P_{CV,\max} = \frac{1 + \mu}{1 + \mu P_{CV}^{-1}(z_0)} . \tag{5}$$

The higher $P_{CV,\max}$, the lower the possibility that a peak in $P_C(z)$ leads to a wrong identification of the ground

scatterer. **Figure 2** shows the behaviour of $P_{CV,\max} / P_{CV}(z_0)$ as a function of $P_{CV}(z_0)$ for different values of the number of images K and $T = 1$, and calculated in the most critical case of $\mu = \mu_{\min}$. Increasing K is beneficial for increasing $P_{CV,\max}$, especially for low values of $P_{CV}(z_0)$. From **Figure 1**, as $P_{CV}(z_0)$ increases, $\mu_{\min}$ decreases. As a consequence, the tolerated level (including the one of the sidelobes caused by the track distribution) decreases, and the increase of the number of images has a negligible effect.

As a final remark, these formulas show that Δz_0, $\mu_{\min}$ and $P_{CV,\max}$ depend on the volume reflectivity profile only through $P_{CV}(z_0)$. Therefore, fixed an acquisition configuration, different volume reflectivity profiles can result into the same ground estimation performance. On the other hand, fixed the volume reflectivity profile, different acquisition configuration can provide different $P_{CV}(z_0)$.

3 Test site and data sets

The experimental analysis has been carried out by processing a L-band TomoSAR airborne acquisition carried out by means of the DLR's F-SAR platform over the Traunstein forest site (south of Germany). The topography ranges from 630 to 720 m above sea level and includes a few areas with steep slopes. Forest top heights range from 10 m up to 45 m. The average biomass level is about 200 Mg/ha and is significantly higher than other managed forests in the same ecological zone (temperate zone). On May 17, 2017, 11 tracks were flown with (nominally) uniformly distributed horizontal displacements between 5 and 50 m. This data set allows to analyze the effect of changing tracks distribution on the TomoSAR height estimates.

The expected TomoSAR imaging performance is primarily affected by the available vertical wavenumbers. The k_Z's obtained from the chosen acquisition are plotted in **Figure 3**. Although they were planned uniformly distributed, in-flight deviations from the planned tracks made the realized ones (slightly) non-uniform. The TomoSAR Rayleigh vertical resolution, which is inversely proportional to the largest k_Z amounts to around 9 m at mid range.

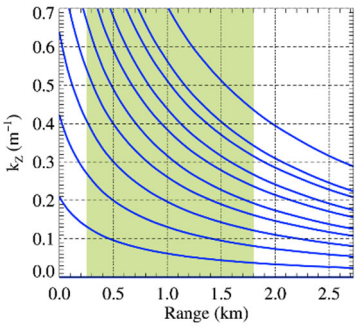

Figure 3 Vertical wavenumbers corresponding to the tracks realized during the TomoSAR acquisition as a function of the range coordinate, and averaged along azimuth. The range coordinate is relative to the (azimuth-variant) range at the processed swath start. The green box indicates the range extension of the area of interest. A null vertical wavenumber is conventionally assigned to the master track.

4 Experimental results

The height estimation performance obtained by the Capon spectral estimator in the estimation of the ground height is is reported in this Section. In particular, the role of the increase of the maximum vertical wavenumber $\max(k_Z)$ (hence the consequential improvement of resolution) is addressed. In this analysis, $\min(k_Z)$ is fixed (hence the TomoSAR height ambiguity) and a (nominally) uniform distribution of k_Z is assumed. Since for uniform tracks it results $\max(k_Z) = (K-1)\cdot\min(k_Z)$, an increase of $\max(k_Z)$ for fixed $\min(k_Z)$ corresponds to an increase of K. In this analysis, K varies between 4 and 11. Interferometric coherences have been estimated on a 15 m × 15 m (slant range-azimuth) multi-look cell, corresponding to approximately 288 independent looks. The estimated heights have been validated against the available lidar topography. As explained in Section 2, $T = 1$ has been set.

The improvement in vertical resolution brought by an increase of K improves the TomoSAR capabilities of separating scattering contributions at different heights. In particular, the capability to separate ground and volume scattering contributions enables a better estimation of the ground height from a TomoSAR profile. This is shown in the HH error maps in **Figure 4**. For $K = 6$ (vertical resolution 18 m) the estimation error is well below 5 m in absolute value across a large part of the aerea of interest. Increasing K to 11 makes the error decrease further especially in shorter stands. Residual larger errors are found in correspondence of large slopes, whose effect can only be counteracted by changing viewing direction.

The ground estimation error is quantified in **Figure 5** as a function of the forest top height in terms of bias and standard deviation. The plots in **Figure 5(a)** refer to the HH polarization channel. Both bias and standard deviation increase with height as the attenuation of the volume increases as well, resulting in a weaker ground. However, their value normalized by the top height decreases. Any vertical resolution improvement reduces both the estimation bias and standard deviation. The best estimates are obtained for $K \geq 9$ (resolution better than 10 m): the bias is lower than or equal to 1 m and independent of height, while the standard deviation increases slower with height than for lower K. In taller stands, the standard deviation can reach around 4 m (10% of the volume height). The estimation error in HV follows the same trend, but with larger values. The ground-to-volume ratio can be improved by optimizing the polarization channel using standard (multi-baseline) Pol-InSAR techniques extended to TomoSAR [1], [9]. The effect of such optimization on the ground height

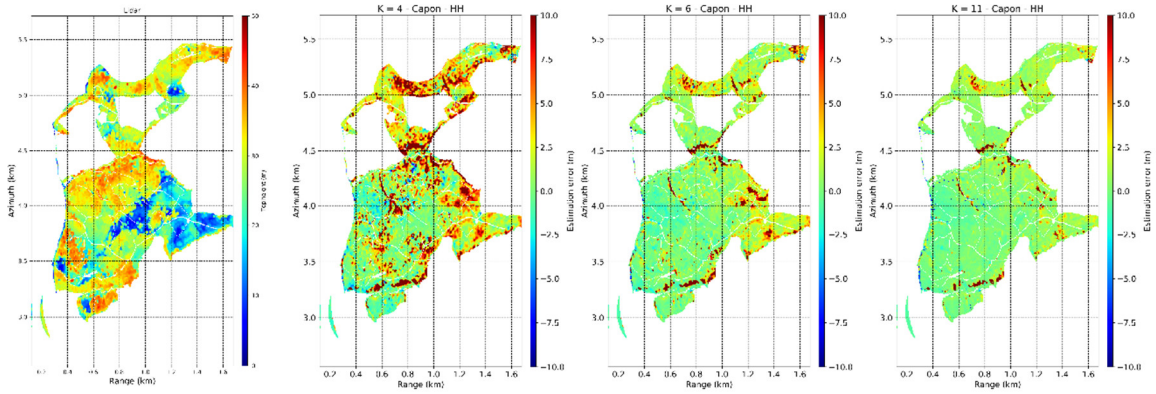

(a) (b) (c) (d)

Figure 4 Traunstein forest: (a) lidar top height and Capon ground height estimation error maps obtained in HH as a function of the number of tracks (vertical resolution) with (b) $K = 4$ (30 m vertical resolution), (c) $K = 6$ (18 m vertical resolution), (d) $K = 11$ (9 m vertical resolution).

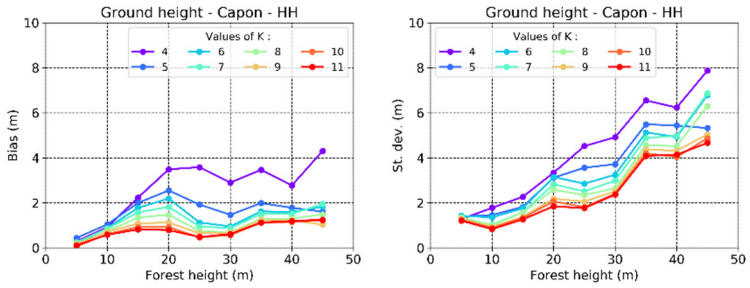

(a)

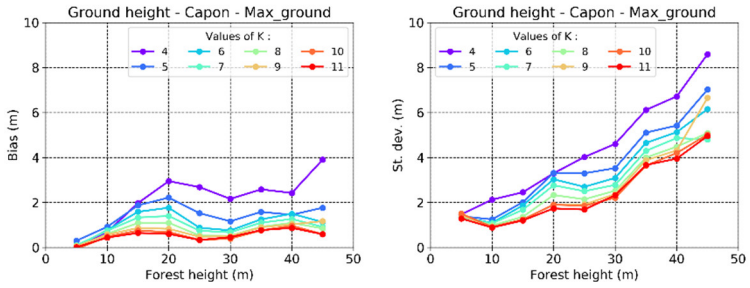

(b)

Figure 5 Traunstein forest, ground height estimation performance (bias and standard deviation) as a function of the forest height (a) for the HH channel, and (b) for the polarization channel with maximum ground-to-volume ratio.

estimation error is quantified in **Figure 5(b)**. The estimation bias decreases with respect to the HH case, especially for lower K (worse vertical resolution). An improvement continues to be present at the increase of K (better vertical resolution), but not so significant. On the same line, it has been seen that the effect of the polarization is larger for instance by using the beamforming spectral estimator, which is characterized by worse resolution capabilities than the Capon estimator.

Finally, **Figure 6(a)** shows the distribution of the ground height estimation error as a function of the ground-to-volume ratio in the polarization channel with maximum ground. The estimation error decreases at the increase of the ground-to-volume ratio, as it is reasonable to expect. Even a low ground-to-volume ratio in the order of -15 dB allows an acceptable estimation performance. However, recalling **Figure 1**, this value of ground-to-volume ratio can limit the ability to detect the ground peak in the Capon profile. As shown by the curves in **Figure 1** and by the error distribution from the real data analysis in **Figure 6(b)**, the contribution at the ground of the volume reflectivity profile makes the ground visible again. Even a small increase of the ground-to-volume ratio pushes the estimation error around 1 m.

5 Conclusions

In this paper, the performance achievable by Capon TomoSAR profiles in the estimation of the ground height

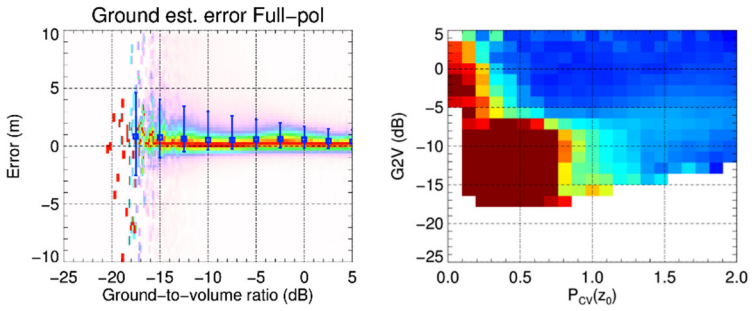

Figure 6 Traunstein forest, distribution of the ground height estimation error in the polarization channels with maximum ground-to-volume ratio and $K = 11$ (a) as a function of the ground-to-volume ratio, and (b) in the plane defined by the Capon power of the volume-only profile in correspondence of the ground, and the ground-to-volume ratio (see also **Figure 1**). The error colorbar ranges between 0 (dark blue) and 5 m (dark red).

has been discussed by means of theoretical relationships and real data experiments. The experiments have been carried out with an L-band TomoSAR data set acquired over a temperate forest.

The derived theoretical relationships are independent of the specific distribution of the acquisition tracks. They show first of all that only the volume scattering contribution in correspondence of the ground affects the ability to detect the presence of ground scattering. Fixed this value and one value of ground-to-volume ratio, also the increase of the number of images in TomoSAR stack improves not only the ability to detect the ground scattering in the profile, but also reduces the possibility that a volume peak or sidelobe is mistaken for the ground peak.

The experimental results have shown that increasing the vertical Rayleigh resolution is critical for achieving a fixed performance. This is not only due to the higher interferometric sensitivity brought by the longer baselines, but also by the increased ability to separate scattering contributions in height. At the same time, the estimation performance depends on the ground-to-volume ratio. In this sense, its maximizations through a polarimetric optimization improve also the ground estimation performance. This improvement becomes more significant for suboptimal vertical resolutions.

6 Literature

[1] S. Cloude, K. Papathanassiou, "Three-stage inversion process for polarimetric SAR interferometry," IEE Proc. – Radar Sonar Navig., vol. 150, no. 3, 125- 134, Jun. 2003.

[2] H. Jörg, M. Pardini, I. Hajnsek, K. Papathanassiou, "On the separation of ground and volume scattering using multibaseline SAR data," IEEE Geosci. Remote Sens. Lett., vol. 14, no. 9, pp. 1570-1574, Sept. 2017.

[3] M. Pardini, K. Papathanassiou, "On the estimation of ground and volume polarimetric covariances in forest scenarios with SAR tomography," IEEE Geosci. Remote Sens. Lett., vol. 14, no. 10, pp. 1860-1864, Oct. 2017.

[4] S. Tebadini, "Single and Multipolarimetric SAR Tomography of Forested Areas: A Parametric Approach," IEEE Trans. Geosci. Remote Sens., vol. 48, no. 5, pp. 2375-2387, May 2010.

[5] M. Pardini, K. Papathanassiou, "Sub-canopy topography estimation: Experiments with multibaseline SAR data at L-band," Proc. of 2012 IEEE Int. Geosci. Remote Sens. Symp., IGARSS 2012, Munich, Germany, pp. 4954-4957, Jul. 2012.

[6] Y. Huang, J. Levy-Vehel, L. Ferro-Famil, A. Reigber, "Three-dimensional imaging of objects concealed below a forest canopy using SAR tomography at L-band and wavelet-based sparse estimation," IEEE Geosci. Remote Sens. Letters, vol. 14, no. 9, pp. 1454-1458, Sept. 2017.

[7] F. Lombardini, M. Pardini, "Experiments of tomography-based SAR techniques with P-band polarimetric data," Proc. 4 th ESA Int. Workshop on Polarimetry and Polarimetric Interferometry, PolInSAR 2009, Frascati, Italy, Jan. 2009

[8] S. Tebaldini, F. Rocca, "Multibaseline polarimetric SAR tomography of a boreal forest at P- and L-bands," IEEE Trans. Geosci. Remote Sens., vol. 50, no. 1, pp. 232-246, Jan. 2012.

[9] M. Pardini, M. Tello, V. Cazcarra-Bes, K. Papathanassiou, I. Hajnsek, "L- and P-band 3-D SAR reflectivity profiles vs. lidar waveforms: The AfriSAR case", IEEE Journal Sel. Topics Applied Earth Obs. Remote Sens., vol. 11, no. 10, pp. 3386-3401, Nov. 2018.

[10] M. Mariotti d'Alessandro, S. Tebaldini, "Digital Terrain Model Retrieval in Tropical Forests Through P-Band SAR Tomography," IEEE Trans. Geosci. Remote Sens., vol. 57, no. 9, pp. 6774-6781, Sep. 2019.

[11] P. Stoica, R. Moses, Spectral Analysis of Signals, Prentice Hall, 2005.

[12] C. Vaidyanathan, K. M. Buckley, "Performance Analysis of the MVDR Spatial Spectrum Estimator," IEEE Trans. Signal Proc., vol. 43, no. 6, pp. 1427-1437, Jun. 1995.